Demonstration of mid-infrared waveguide photonic crystal cavities

Hongtao Lin,[1] Lan Li,[1] Fei Deng,[1] Chaoying Ni,[1] Sylvain Danto,[2] J. David Musgraves,[3] Kathleen Richardson,[2] and Juejun Hu[1,*]

[1]*Department of Materials Science & Engineering, University of Delaware, Newark, Delaware 19716, USA*

[2]*College of Optics & Photonics, Department of Materials Science and Engineering, University of Central Florida, Orlando, Florida 32816, USA*

[3]*IRradiance Glass Inc., Orlando, Florida 32828, USA*

Corresponding author: hujuejun@udel.edu

We have demonstrated what we believe to be the first waveguide photonic crystal cavity operating in the mid-infrared. The devices were fabricated from $Ge_{23}Sb_7S_{70}$ chalcogenide glass (ChG) on CaF_2 substrates by combing photolithographic patterning and focused ion beam milling. The waveguide-coupled cavities were characterized using a fiber end fire coupling method at 5.2 μm wavelength, and a loaded quality factor of ~2000 was measured near the critical coupling regime. © 2013 Optical Society of America

OCIS codes: (130.5296) Photonic crystal waveguides; (230.5750) Resonators; (130.3060) Infrared.
http://dx.doi.org/10.1364/OL.38.002779

Waveguide microbeam/nanobeam photonic crystal (PhC) cavities have become promising alternatives to conventional cavity geometries [1,2]. Quality (Q) factors up to 10^6 have been achieved in these 1D cavities through a Bloch mode engineering design approach [3]. Coupled with their small mode volume, waveguide PhC cavities are recognized as ideal platforms for exploring cavity-enhanced photon–matter interactions given their high cavity finesse [4]. In addition, waveguide PhC cavities are inherently amenable to integration with traditional index-guided waveguides, an important advantage for planar photonic integration. To date, waveguide PhC cavities have only been characterized at visible or near-infrared (near 1550 nm) wavelengths [5–9]. Waveguide PhC cavity devices operating in the mid-infrared (mid-IR, 3–20 μm wavelengths), a strategically important wave band for spectroscopic sensing, free-space communications, and thermal imaging [10], have not yet been demonstrated.

A main technical challenge to mid-IR photonic device fabrication is the much limited material choices. The conventional optical cladding material, silica, becomes opaque at wavelengths longer than 3.5 μm. As a consequence, mid-IR devices demonstrated to date almost exclusively rely on wafer bonding to mid-IR transparent substrates (e.g., sapphire [11–13] or silicon nitride [14]) or suspended structures [15–19], which significantly complicate device fabrication and integration. Here we explore an alternative device design based on amorphous ChGs. These glass materials are well known for their broad transparency in the mid-IR range [20]. Furthermore, their amorphous structure enables direct monolithic integration on virtually any substrates free of lattice matching constraints. Finally, ChGs possess a photothermal figure of merit 100 times higher than those of silica and silicon, making them ideal material candidates for ultrasensitive photothermal spectroscopic sensing applications [21,22], where mid-IR waveguide PhC cavities constitute the basic device building block. Recently, we have demonstrated ChG resonators on silicon with a high intrinsic Q factor of 2×10^5

in the mid-IR following the monolithic integration approach [23].

In this Letter, we discuss the first experimental demonstration of mid-IR 1D waveguide PhC cavities. The cavities were made of $Ge_{23}Sb_7S_{70}$ ChGs, and were monolithically fabricated on mid-IR transparent CaF_2 substrates. The $Ge_{23}Sb_7S_{70}$ glass is transparent up to 12 μm wavelength, and is stable against moisture, oxidation, and acid solutions. The combination of a high-index $Ge_{23}Sb_7S_{70}$ glass ($n = 2.2$) waveguide core and a low-refractive-index CaF_2 substrate ($n = 1.4$) offers large index contrast for strong optical confinement in the cavities.

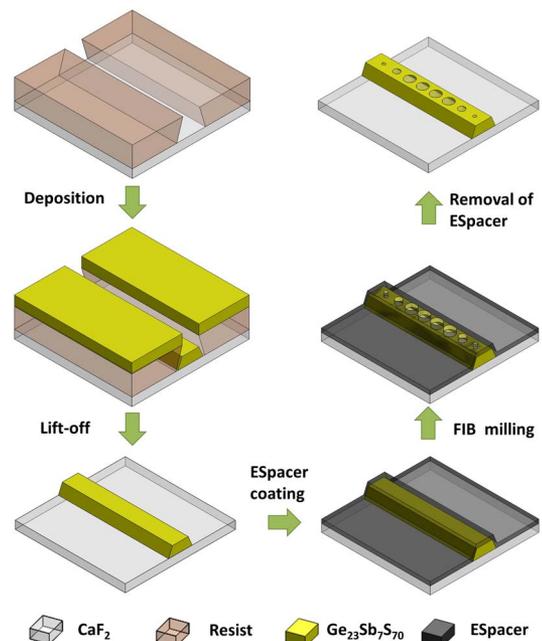Figure 1 schematically illustrates the fabrication process flow of the 1D waveguide PhC cavity. The $Ge_{23}Sb_7S_{70}$

Fig. 1. Schematic fabrication process flow for the $Ge_{23}Sb_7S_{70}$ ChG waveguide PhC cavities on CaF_2.

glass films were first deposited on 1″ (111) CaF$_2$ substrates (Shanghai Daheng Optics and Fine Mechanics) via thermal evaporation. The glass films show excellent adhesion with the CaF$_2$ substrates, and no film delamination was observed during subsequent processing. The PhC microbeam was fabricated using a two-step process combining UV lithography and focused ion beam (FIB) milling. Instead of sculpting the entire structure using FIB, the two-step process minimizes the milling area and improves fabrication throughput. Details of the glass film deposition and lithographic patterning processes can be found elsewhere [24,25]. After fabrication of 3 μm wide, 1.2 μm thick single-mode waveguide devices, a layer of 20 nm thick water-soluble conducting polymer (Espacer, Showa Denko) was spin coated onto the substrate to prevent charging [26,27] during ion beam milling. The PhC holes were defined by a Ga^{2+} ion beam (beam current 20 pA, accelerating voltage 30 kV) using a Zeiss Auriga 60 CrossBeam FIB nanoprototyping workstation. After milling, the PhCs were rinsed in deionized water to remove the Espacer layer and complete the device fabrication.

Figure 2(a) provides an SEM anatomy view of holes etched by FIB. From left to right, the milling doses were linearly increased from 0.2 to 1.2 nC/μm^2. The etch depths linearly increase with the etch dose [Fig. 2(c)], and the effective etch yield is about 1.2 μm^3/nC. We also note that CaF$_2$ serves as an excellent etch stop to Ga^{2+} ion milling, which allows precise definition of the PhC hole depth. A close view in Fig. 2(b) clearly shows that there is little re-deposition of glass on the hole sidewalls, yielding a high-quality, smooth surface finish.

The fabricated cavity geometry consists of a segment of glass waveguide sandwiched between two identical PhC mirror reflectors milled at 0.4 nC/μm^2 ion beam dose. Figure 2(d) presents an optical microscope top-view image of the cavity structure, and Fig. 2(e) shows an SEM top view of one of the PhC mirrors. We chose Fabry–Perot cavity designs with a long cavity length in this initial demonstration to facilitate isolation and quantification of optical loss mechanisms in the cavity, since the mirror strength (reflectance) and extrinsic cavity Q factor can be readily tuned by changing the number of holes making up the mirrors. To minimize optical scattering loss, five size-tapered holes are inserted at both sides of the PhC mirror. The diameter of PhC mirror holes was fixed at 1.2 μm, and the diameters of the five taper holes were linearly decreased from 1 to 0.2 μm, as illustrated in Fig. 2(f). Our numerical simulations indicate a reduction of single-bounce scattering loss from 4% to 0.5% though incorporation of the taper structure.

We fabricated two types of cavities with cavity lengths of 170 and 440 μm, respectively. The hole period for both types of cavities was 1.65 μm, which creates a photonic band edge near 5.2 μm wavelength. Strong wavelength dependence of PhC mirror reflectance is thus expected in the wavelength regime near the band edge, leading to significant reduction of the cavity Q factor as the resonant wavelength approaches the band edge. Figure 3 plots transmission and reflection spectra of a waveguide PhC mirror with a period of 1.65 μm simulated using the finite-difference time-domain (FDTD) technique [28]. It can be seen that the PhC mirror strength decreases at

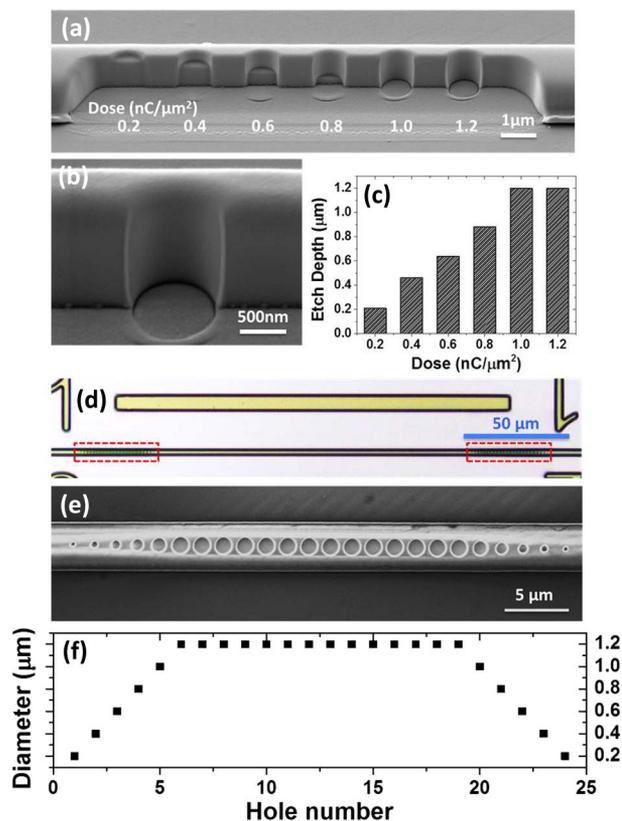Fig. 2. (a) Anatomy section of holes in a 3 μm wide, 1.2 μm thick Ge$_{23}$Sb$_7$S$_{70}$ ChG waveguide milled using different ion beam dose for etch rate calibration; (b) cross-sectional SEM image of a PhC through hole, showing a smooth surface finish and near vertical sidewalls; (c) FIB etch depth of the holes plotted as a function of ion beam dose inferred from panel a (the CaF$_2$ substrate serves as an excellent etch stop for FIB milling, and thus the etch depth saturates at the glass film thickness); (d) top-view microscope image of waveguide PhC cavity, consisting of a section of unstructured channel waveguides (~170 μm in length) confined between two PhC mirrors (marked by the red boxes); (e) top-view SEM image of one of the PhC mirrors; (f) diameters of PhC mirror holes shown in panel (e) (the center-to-center spacing between the holes is fixed at 1.65 μm).

longer wavelengths, manifesting the PhC band edge effect. On the other hand, in the spectral regime near the center of the photonic band gap, little wavelength dependence of the cavity Q factor is expected, and the mirror strength can be effectively tuned by changing the number of PhC holes: increasing the hole number leads to high mirror reflectance and an increase of the extrinsic cavity Q factor.

These general characteristics of the PhC cavities were validated through transmission measurements of the PhC cavities. The measurements were performed on a homebuilt fiber end fire coupling system. Details of the experimental setup and measurement method were discussed in our previous work [23]. Figure 4(a) shows the transmission spectrum of a waveguide PhC cavity with a cavity length of 170 μm and 14 PhC mirror holes. Multiple longitudinal orders of cavity resonances were clearly visible from the spectrum. The loaded cavity Q factors of these resonances monotonically decrease from 1300 to 400 as the resonant wavelength approaches the photonic
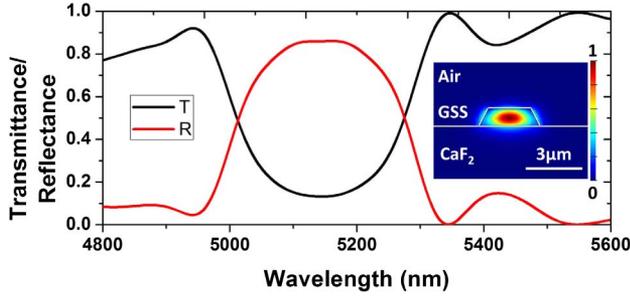
Fig. 3. Simulated transmission and reflection spectra of the PhC mirror in Fig. 2(e). Inset shows the TE mode intensity profile of the unstructured mid-IR glass waveguide.

band edge [Fig. 4(b)], which agrees well with our simulation results and unequivocally confirms the photonic band gap effect in our fabricated structures.

To further assess the loss mechanisms in the waveguide PhC cavities, a series of cavities with different PhC mirror hole numbers were fabricated and tested. As we expected, the Q factors show minimal wavelength dependence, the level of the dependence being completely overshadowed by our experimental measurement uncertainty. Figure 5(a) plots the transmission spectrum of a PhC cavity with 10-hole mirror sets. Figure 5(b) compares the experimentally measured and numerically simulated quality factors as the PhC mirror hole number is varied. The measured Q factors were averaged from at least seven resonance peaks near the center of the photonic stop band. The figure shows monotonic
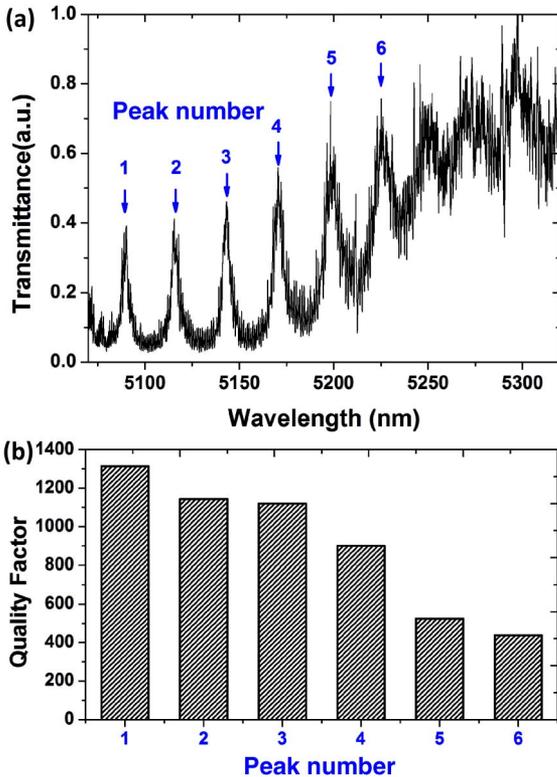

Fig. 4. (a) Mid-IR optical transmission spectrum of the waveguide PhC cavity shown in Fig. 2(d) (cavity length 170 μm, 14 PhC mirror holes) measured using a wavelength sweeping method; (b) quality factor of resonance peaks in panel (a)—their Q factors monotonically decrease as their resonant wavelengths approach the photonic band edge.
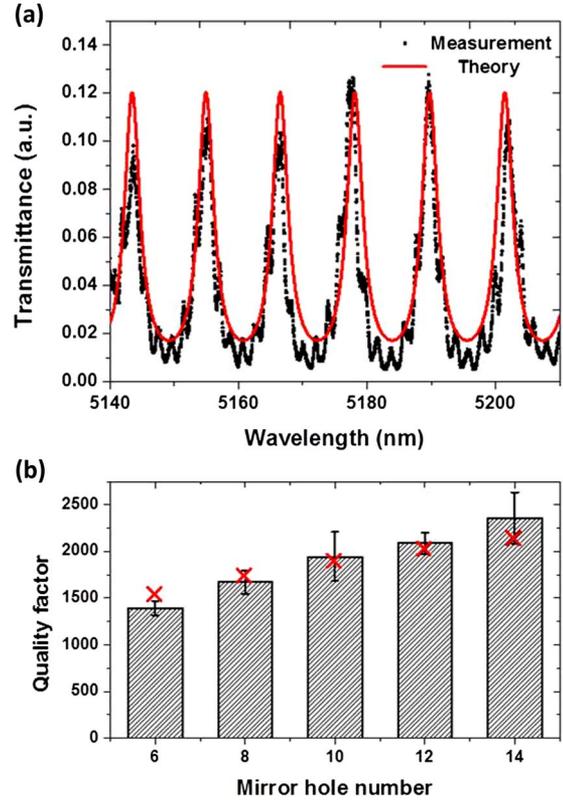

Fig. 5. (a) Mid-IR transmission spectrum of a waveguide PhC cavity with a 440 μm long cavity positioned between two 10-hole PhC mirrors; (b) evolution of loaded cavity Q factors as the PhC mirror hole number increases: the black bars represent experimentally measured Q values, and the red crosses denote simulation results using the fitted waveguide optical loss value (53 dB/cm) in Table 1.

increase of the loaded cavity Q factor as the mirror hole number increases, which is an anticipated result since the external Q factor scales with cavity mirror strength. The waveguide loss (53 ± 4 dB/cm) was first fitted from the measured Q factors and extinction ratios of the five devices. The loss value and FDTD simulated parameters listed in Table 1 were then used to calculate the transmission spectrum shown in Fig. 5(a) based on the following equation:

$$T = \left| \frac{T_s \exp(ikL - 0.5\alpha L)}{1 - R_s \exp(2ikL - \alpha L)} \right|^2,$$

where T is the total transmittance through the cavity, T_s and R_s are the mirror transmittance and reflectance values derived from FDTD simulations, α represents the optical loss, which includes both waveguide propagation loss and scattering loss of the mirrors, L gives the

Table 1. Parameters Used to Calculate the PhC Cavity Transmittance in Fig. 5(a)

T_s	R_s	n_{eff}
0.2463	0.7489	1.6524
n_g	α	L (μm)
2.6083	53 dB/cm	442

cavity length, and k denotes the wave vector and is defined by $k = 2\pi n_{eff}/\lambda$. The wavelength-dependent waveguide effective index n_{eff} can be obtained from modal simulations. The high optical loss ($\alpha = 53$ dB/cm), which accounts for the relatively low cavity Q, may be attributed to scattering loss resulting from waveguide sidewall roughness and the PhC mirrors. Further improvement of the waveguide PhC cavity Q factors is expected through processing optimization and new designs following a deterministic PhC cavity optimization strategy [29]: for example, we have designed and numerically simulated a ChG PhC microbeam cavity with a loaded Q as high as 10^6 [22].

In conclusion, we have shown, to the best of our knowledge, the first demonstration of mid-IR waveguide PhC cavities. The cavity devices are made of $Ge_{23}Sb_7S_{70}$ ChG on CaF_2 substrate using a two-step patterning process combining lithography and FIB milling techniques. The devices exhibit a loaded quality factor of ∼2000, and an extinction ratio up to 13 dB near the critical coupling operation regime at the mid-IR wavelength of 5.2 μm. The PhC cavity device platform can potentially serve as a useful building block for applications including on-chip chemical sensing, optical free-space communications, and thermal imaging.

References

1. J. S. Foresi, P. R. Villeneuve, J. Ferrera, E. R. Thoen, G. Steinmeyer, S. Fan, J. D. Joannopoulos, L. C. Kimerling, H. I. Smith, and E. P. Ippen, Nature **390**, 143 (1997).
2. K. J. Vahala, Nature **424**, 839 (2003).
3. P. Lalanne and J. P. Hugonin, IEEE J. Quantum Electron. **39**, 1430 (2003).
4. M. Notomi, E. Kuramochi, and H. Taniyama, Opt. Express **16**, 11095 (2008).
5. P. Velha, E. Picard, T. Charvolin, E. Hadji, J. C. Rodier, P. Lalanne, and D. Peyrade, Opt. Express **15**, 16090 (2007).
6. P. B. Deotare, M. W. McCutcheon, I. W. Frank, M. Khan, and M. Loncar, Appl. Phys. Lett. **94**, 121106 (2009).
7. Q. Quan, P. B. Deotare, and M. Loncar, Appl. Phys. Lett. **96**, 203102 (2010).
8. W. H. P. Pernice, C. Xiong, C. Schuck, and H. X. Tang, Appl. Phys. Lett. **100**, 091105 (2012).
9. M. Eichenfield, J. Chan, R. M. Camacho, K. J. Vahala, and O. Painter, Nature **462**, 78 (2009).
10. R. A. Soref, Proc. SPIE **6898**, 689809 (2008).
11. A. Spott, Y. Liu, T. Baehr-Jones, R. Ilic, and M. Hochberg, Appl. Phys. Lett. **97**, 213501 (2010).
12. C. Y. Wong, Z. Cheng, X. Chen, K. Xu, C. K. Fung, Y. M. Chen, and H. K. Tsang, IEEE Photon. J. **4**, 1095 (2012).
13. R. Shankar, I. Bulu, and M. Loncar, Appl. Phys. Lett. **102**, 051108 (2013).
14. S. Khan, J. Chiles, J. Ma, and S. Fathpour, Appl. Phys. Lett. **102**, 091105 (2012).
15. R. Shankar, R. Leijssen, I. Bulu, and M. Loncar, Opt. Express **19**, 5579 (2011).
16. R. Shankar, I. Bulu, R. Leijssen, and M. Loncar, Opt. Express **19**, 24828 (2011).
17. Z. Cheng, X. Chen, C. Y. Wong, K. Xu, and H. K. Tsang, IEEE Photon. J. **4**, 1510 (2012).
18. Y. Xia, C. Qiu, X. Zhang, W. Gao, J. Shu, and Q. Xu, Opt. Lett. **38**, 1122 (2013).
19. C. Reimer, M. Nedeljkovic, D. J. M. Stothard, M. O. S. Esnault, C. Reardon, L. O'Faolain, M. Dunn, G. Z. Mashanovich, and T. F. Krauss, Opt. Express **20**, 29361 (2012).
20. A. Seddon, J. Non-Cryst. Solids **184**, 44 (1995).
21. J. J. Hu, Opt. Express **18**, 22174 (2010).
22. H. Lin, Z. Yi, and J. Hu, Opt. Lett. **37**, 1304 (2012).
23. H. Lin, L. Li, Y. Zou, S. Danto, J. D. Musgraves, K. Richardson, S. Kozacik, M. Murakowski, D. Prather, P. T. Lin, V. Singh, A. Agarwal, L. C. Kimerling, and J. Hu, Opt. Lett. **38**, 1470 (2013).
24. L. Petit, N. Carlie, F. Adamietz, M. Couzi, V. Rodriguez, and K. C. Richardson, Mater. Chem. Phys. **97**, 64 (2006).
25. J. J. Hu, V. Tarasov, A. Agarwal, L. Kimerling, N. Carlie, L. Petit, and K. Richardson, Opt. Express **15**, 2307 (2007).
26. D. Freeman, S. Madden, and B. Luther-Davies, Opt. Express **13**, 3079 (2005).
27. C. Grillet, C. L. C. Smith, D. Freeman, S. Madden, B. Luther-Davies, E. Magi, D. Moss, and B. Eggleton, Opt. Express **14**, 1070 (2006).
28. http://www.lumerical.com.
29. Q. M. Quan and M. Loncar, Opt. Express **19**, 18529 (2011).